Unveiling the electronic origin of lanthanide based Metal Organic Framework with ideal spin filtering capacity

Check for updates

Xuban Gastearena [1], Jesus M. Ugalde [1,2], German E. Pieslinger [2,3], Eider San Sebastian [4] ✉ & Elisa Jimenez-Izal [1,2] ✉

Recently, a three dimensional metal-organic framework (MOF) based on Dy(III) and the L-tartrate ligand was experimentally shown to exhibit a spin polarization (SP) power of 100% at room temperature. The material's spin filtering ability was ascribed to the chiral-induced spin selectivity (CISS) effect. In this work, we computationally characterize the electronic structure of this MOF, revealing that the high SP of the material is linked to the asymmetric arrangement, around the Fermi level, of the alpha- and beta-spin electron states arising from the 4f-states of the lanthanide Dy atom, which results in two different conduction channels (band gaps) for each spin state. Based on the understanding gathered in this work, we propose that the substitution of the hydroxyl groups of the ligand by mercaptan groups should boost the electrical conductivity, while retaining the spin filtering power of the material.

Spin-polarized electron currents (SPECs), where the proportion of electrons of one spin is larger than the other, are of major importance due to their applicability in spintronics[1] (data storage devices, sensors, etc.) and in spin-dependent physical-chemical processes[2,3] (water electrolysis, organic photovoltaics, etc.). However, very few filtering materials capable of generating SPEC of high intensity are known. The few ones characterized up-to-date, featured with high spin–orbit coupling (SOC) ferromagnetic materials, based on transition metal ferromagnets or their alloys. Nevertheless, these materials usually exhibit only a moderate spin polarization (SP)[4] of around 45%.

Recently, since the discovery of the chirality-induced spin selectivity (CISS) effect[5] in 2012 it is now well established that chiral molecules can act as spin-filtering materials[6–9], namely, they conduct preferentially electrons of one spin over the other, in processes involving electron transfer, transport, and transmission. In this vein, recently, the SP power of an enantiomerically pure 3D chiral Metal Organic framework (MOF) based on Dy(III) ions and L-2,3-dihydroxybutanediate as coordinating ligand (herein L-tartrate), belonging to the chiral and non-centrosymmetric P-1 triclinic space group (Supplementary Note 1 and Supplementary Fig. 1) was reported to be 100% at room temperature[10]. The highest SP power reported up-to-date for

molecular systems. Earlier reports for the SP power of self-assembled chiral monolayers made of helical DNA[11,12], oligopeptides[13], helicenes[14], and cysteine-capped-CdSe chiral quantum dots[15], or a 2D lead-iodide-based perovskite[16], were within the 40–85% range. The recently synthesized lanthanide containing chiral metallopeptides[17], highlight that the inclusion of paramagnetic atomic centers enhances the spin polarization power of molecular systems.

The spin-filtering ability of the chiral 3D Dy-L MOF was tentatively ascribed to the CISS effect, arising from the coupling between the chirality and helicity of the material with the magnetic dipole of the transmitted electrons, enhanced by the large SOC effect of the Dy(III) ions. Furthermore, this MOF behaved as a semiconductor for the transmitted electrons with a measured bandgap of 1.15 eV.

In this communication, we report a thorough investigation of the electronic structure of our 3D Dy-L MOF. We found an asymmetric arrangement of the electronic states of its alpha- and beta-spin electrons around the Fermi energy, featuring different band gaps for each electronic spin. Moreover, by analyzing the electronic structure of an analogous non-chiral but centrosymmetric 3D Dy MOF, the helicity (or chirality of the

[1]Polimero eta Material Aurreratuak: Fisika, Kimika eta Teknologia Saila, Kimika Fakultatea, Euskal Herriko Unibertsitatea (UPV/EHU), Donostia, Euskadi, Spain. [2]Donostia International Physics Center (DIPC), M. de Lardizabal Pasealekua 3, Donostia, Euskadi, Spain. [3]CONICET—Universidad de Buenos Aires, Instituto de Química y Fisicoquímica Biológicas (IQUIFIB), Buenos Aires, Argentina. [4]Kimika Aplikatua Saila, Kimika Fakultatea, Euskal Herriko Unibertsitatea (UPV/EHU), Donostia, Euskadi, Spain. ✉e-mail: eider.sansebastian@ehu.eus; elisa.jimenez@ehu.es

space group) of the system is ruled out as an essential factor for the spin-filtering capacity. Finally, we propose that the second generation of conducting spin-filtering 3D-MOFs, should be engineered with sulfur-based tartrate derivative bridging ligands in order to yield stronger covalent interactions with the metal, since they are known to boost electric conductivity via the through-bond charge delocalization[18,19]. Such materials are predicted to show structural integrity, enhanced conductivity and yet, 100% spin polarizability power.

Results and discussion

The geometry of the 3D Dy-L-Tar MOF was optimized using PBE-D3 and placing the f electrons of the lanthanide in the pseudopotential. The unit cell contains 62 atoms, including 2 Dy^{3+} ions that are nonacoordinated to the oxygen atoms of surrounding L-tartrate and water molecules (see Supplementary Note 5 and Supplementary Fig. 5). Upon geometry optimization, the electronic structure was computed with the HSE06-D3 functional and explicitly treating the f electrons of Dy^{3+}. The most stable electronic configuration was found to have ten unpaired electrons per unit cell, with five unpaired electrons located on each Dy atom.

The computed PDOS of the 3D Dy-L-Tar MOF is shown in Fig. 1. The Fermi level corresponds to the fully polarized beta-spin electronic states arising from the 4f orbitals of the Dy ion. Furthermore, notice the asymmetrical arrangement of the alpha and beta electronic states around the Fermi energy level. Alpha electrons could be only conducted between the occupied and unoccupied p states of the ligands' oxygen atoms, by surpassing an energy gap of 6.25 eV. For the beta electrons, we believe that our system behaves similarly to extrinsic semiconductors where the states introduced by the impurity (dopant or defect) at the Fermi level are responsible for the insulator-semiconductor transition by lowering the bandgap and therefore enhancing the conductivity. Such is the case of the transition metal oxides, for example, the well-studied NiO[20,21]. Analogous behavior has also been claimed for Li-ion battery cathode materials[22]. In our case, the origin of those impurity levels is not temperature, pressure, doping, or defect-induced, but inherent to the material, due to the splitting of the f orbitals in the nonagonal crystal field[23]. Moreover, those states belong to a unique type of spin, lowering only one of the band gaps (for beta-spin electrons) while maintaining the barrier for alpha electrons unaffected. In this manner, the 4f asymmetric states are responsible for both the SF ability (as suggested for EuO, or EuS)[24–26] of the material as well as for the semiconductor behavior for beta electrons and insulator behavior for alpha electrons, in line with experimental measurements. In addition, we cannot rule out that the conductivity is affected by the strongly localized magnetic moment by opposing a higher resistance to alpha spin electrons[27,28]. In this way, the conductivity is affected by two factors: the number of carriers related with the accessible vacant states and the proximity of the valence band (1.25 eV from ligands' 2p to the 4f states, Fig. 1) that regulates the contribution to the conductivity via charge-transfer transitions[29–32].

Importantly, in this work we additionally determined experimentally the electronic bandgap of the 3D Dy-L-Tar MOF, following a standard electrochemical characterization protocol as explained in the Supplementary Information, Note 9. The experimental value for the bandgap is 1.15 eV (see Supplementary Note 9 and Supplementary Fig. 10), which is in perfect agreement with the computed band gap value obtained using DFT calculations. Furthermore, the calculated band gaps of 1.25 eV for beta electrons and 6.25 eV for alpha electrons are aligned with the previously experimentally measured conductivity values of 2.9×10^{-7} S/cm for one spin component electrons and 2.2×10^{-10} S/cm for the opposite spin electrons, since the latter values fall within the typical ranges for semiconductors and insulators, respectively[10,33–35].

Consequently, we propose that the experimentally observed outstanding spin-filtering capacity of this material has its origin in the spin asymmetry near the fermi energy arising from the 4f states of the lanthanide, and this implies that the conducting electrons, only beta-spin electrons, are transmitted through Dy 4f band.

Effect of the chirality of the space group

In order to determine the influence of the fact that 3D Dy-L-Tar MOF is non-centrosymmetric and belongs to a chiral space group in the generation or enlargement of the spin asymmetry of 4f states, the electronic structure of a centrosymmetric 3D Dy MOF which does not belong to any chiral space group was characterized. Specifically, the PDOS of a previously reported 3D MOF based on Dy(III) atoms and the achiral ligand 9,10-anthracenedicarboxylic acid[36] (see Supplementary Note 6 and Supplementary Fig. 6 for crystal structure) was computed and depicted in Fig. 2. As in the previous case, this MOF (which crystallizes in the non-centrosymmetric P-1 space group), shows a spin asymmetry of the 4f states of the Dy metal. Moreover, the shape and f–f distance of the f states of the achiral MOF are the same as in the original chiral 3D Dy-L MOF. This feature can be understood considering that the f states of the lanthanide metal are very localized and do not interact strongly with the ligands. Our results indicate that the spin asymmetry on the lanthanide's 4f states is independent of the chirality of the space group of the material. Nevertheless, notice that in this case the conduction and the valence band are not composed of the 4f states of Dy, and thus no spin-filtering ability is expected in the electron transmission (conductivity) for this material because spin symmetry is not preserved at the Fermi level.

Effect of the softness/hardness of the ligand atoms

Although the 3D Dy-L-Tar MOF was proven to exhibit an outstanding spin-filtering ability with a spin polarization of 100%, it is a poor conductor. The latter might be a consequence of the large ionicity of the chemical bond between Dy^{3+} and the hard oxygens of the carboxylates of the tartrate ligands, a fact which is usually related to insulating behavior. With the aim of identifying the key features of second-generation MOFs with enhanced electrical conductivity retaining 100% spin-filtering capacity, we tested the effect of substituting various oxygen atoms of the L-tartrate ligand by the softer sulfur atom. Such strategy has indeed been proven successful for various similar conducting MOFs, as reviewed recently by Xie et al.[37]. We envisaged five alternative MOFs represented in Fig. 3 along with the original structure (Fig. 3a). In these MOFs, a reduction in the electronic band gap is expected due to a larger through-bond charge delocalization due to an increase in the covalent character of the metal-ligand chemical bond. In this vein, inspection of the atomic Bader charges (see Supplementary Note 7 and Supplementary Fig. 7) reveals that oxygen thiolation of 3D Dy-L-Tar leads to the atomic charge equalization of the Dy-S bonds as compared to the Dy-O ones, indicative of an increased covalent character of the former bonds.

The thiolated tartrate ligands shown in Fig. 3 include the oxygen substitution from the structure shown in Fig. 3a by sulfur atoms of either: all (six) oxygen atoms in the structure (L-6S-Tar, Fig. 3b), all (four) hydroxylic oxygen atoms (L-4Sa-Tar, Fig. 3c), all (four) carboxylic oxygen atoms (L-4Sb-Tar, Fig. 3d), only carboxylic hydroxyl oxygen atoms (L-2Sa-Tar, Fig. 3e) or only chiral-center bound hydroxylic oxygen atoms (L-2Sb-Tar, Fig. 3f). The mentioned thiolated ligands, yielded five computationally generated 3D-MOFs (3D-Dy-L-6S-Tar, 3D-Dy-L-4S-Tar, 3D-Dy-L-4Sb-Tar, 3D-Dy-L-2Sa-Tar, and 3D-Dy-L-2Sb-Tar), whose structures were optimized and the corresponding PDOSs computed as described before and shown in Fig. 4.

The optimization of the geometry of the MOFs based on L-4Sa-Tar, L-2Sa-Tar and L-2Sb-Tar yielded isostructural materials with minor changes in the bond distances around the metal (see Supplementary Note 10, Supplementary Table 2, and Supplementary Fig. 11). On the contrary, and considering the large oxophylicity and low thiophilicity of Dy(III) ions[38], as well as their preferential coordination to carboxylate oxygens as opposed to hydroxyl oxygen atoms (see Supplementary Fig. 6), thiolation of all carboxylic oxygen atoms in L-6S-Tar and L-4Sb-Tar destabilized the 3D lattice of the corresponding MOFs and were therefore excluded from further analysis (see Supplementary Note 8, Supplementary Figs. 8 and 9 of the Supplementary Information).

In the case of 3D-Dy-L-4Sa-Tar and 3D-Dy-L-2Sa-Tar, their PDOS (Fig. 4a, b) revealed the disappearance of the electronic band gap for the beta

electrons leading to a single non-polarized band gap of 2.50 and 3.50 eV, respectively, defined by the p states of the S atoms.

The electronic bandgap for the material with the ligand containing 4S atoms (2.50 eV) is smaller than the one for the ligand with 2S atoms (3.50 eV) as expected for the larger number of softer atoms in the
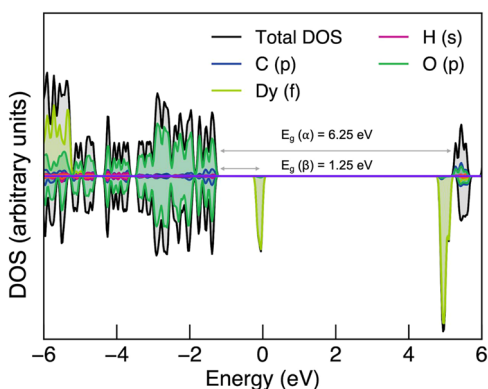

Fig. 1 | Projected density of states (PDOS) of the 3D Dy-L MOF. The zero-energy corresponds to the Fermi level. Alpha spin states are shown above the horizontal line and beta-spin states below. The projected DOS into the p states of C, f states of Dy, s states of H, p states of O and total states are shown in blue, yellow, magenta, green, and black, respectively.
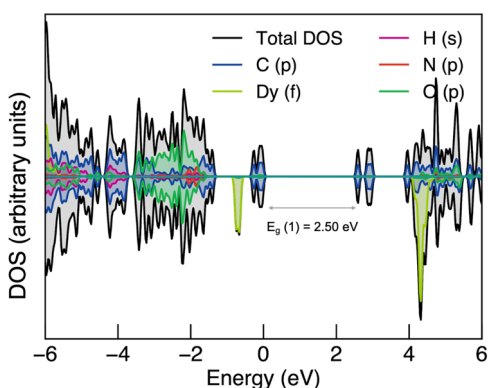
Fig. 2 | The projected density of states (PDOS) of the non-chiral (space group) and non-centrosymmetric 3D Dy MOF. The zero-energy corresponds to the Fermi level. Alpha spin states are shown above the horizontal line and beta-spin states below. The projected DOS into the p states of C, f states of Dy, s states of H, p states of N, p states of O and total states are shown in blue, yellow, magenta, red, green, and black, respectively.

structure. Also, even if the spin asymmetry of the dysprosium 4f states remains, we found that the conduction bands and valence band edges are not composed of such states, which suggests that even though the conduction might be larger, electrons would travel from occupied to unoccupied p states of the S atoms, which are not spin-polarized, and therefore no SP capability is foreseen. On the contrary, inspection of the PDOS of 3D-Dy-L-2Sb-Tar (Fig. 4c), with only two sulfur atoms, reveals that the edge of the conduction band is composed of the beta 4f states of dysprosium. Although the electronic band gap for alpha electrons remains in the range of insulators, e.g., 5.55 eV vs 6.25 eV of the unthiolated one, the band gap for beta electrons is reduced from the 1.25 eV of the unthiolated 3D Dy-L-Tar to 0.55 eV in 3D-Dy-L-2Sb-Tar, suggesting that the latter MOF should behave as a low bandgap semiconductor. Such a reduction is a consequence of the presence of the p states of the S atoms between the oxygen's p and dysprosium's f states. Hence, we propose that the 3D chiral MOF based on Dy(III) atoms and L-2Sb-Tar (L-2,3-dimercapto-succinate) as ligands will exhibit an enhanced conductivity for the beta-spin electrons with respect to its 3D-Dy-L-Tar MOF precursor, without compromising the 100% spin-filtering ability and its structural integrity. The reduction of the bandgap arising from the dysprosium 4f orbitals to 0.55 eV in 3D-Dy-L-2Sb-Tar with respect to 3D-Dy-L-Tar, and considering that the number of hole carriers is unaltered, will enhance the overall conductivity of the former MOF.

All in all, our results suggest that the asymmetric arrangement, around the Fermi level, of the alpha- and beta-spin electron states arising from the f states of the lanthanide Dy atom, can produce spin-filtering properties and has its origin in the lanthanide metal, although the final electronic properties of the MOF will be largely dictated by the ligands.

Conclusions

Recent experimental work has demonstrated that the Dy-L-Tar MOF exhibits an ideal spin-filtering ability with a SP power close to 100% at room temperature. Although such a spin-filtering ability was ascribed to the chirality of the material, an alternative explanation is proposed based on the theoretical electronic structure of the material. In particular, an asymmetric arrangement of alpha and beta-spin states is observed around the Fermi energy, which arises from the 4f states of the lanthanide. As a consequence, electrons of different spin have to overcome different band gaps to be transmitted through the material. This accounts for the semiconductor and insulator behavior of electrons of different spin. Importantly, the calculated band gaps of 1.25 eV for beta electrons (in the range of semiconductors) and 6.25 eV for alpha electrons (in the range of insulators) is in full agreement with the experimentally measured conductivity values of 2.9×10^{-7} S/cm for one spin component electrons and 2.2×10^{-10} S/cm for the opposite spin electrons. Our results point to the spin-polarized electronic states of 3D Dy-L-Tar MOF, around the Fermi level, to be at least partly responsible for the unique electron spin-filtering ability of the material. Furthermore, we show that the chirality of the

Fig. 3 | Chemical structure of different ligands explored in this work. a L-tartaric acid (L-Tar); **b** 2,3-dithio-butanebis (dithioic) acid (L-6S-Tar); **c** 2,3-dimercapto-L-butanebis(thioic) acid (L-4Sa-Tar); **d** 2,3-dihydroxybutanebis(dithioic) acid (L-4Sb-tar); **e** 2,3-dihydroxybutanebis(thioic) O,O-acid (L-2Sa-Tar); **f** 2,3-dimercaptosuccinic acid (L-2Sb-Tar).
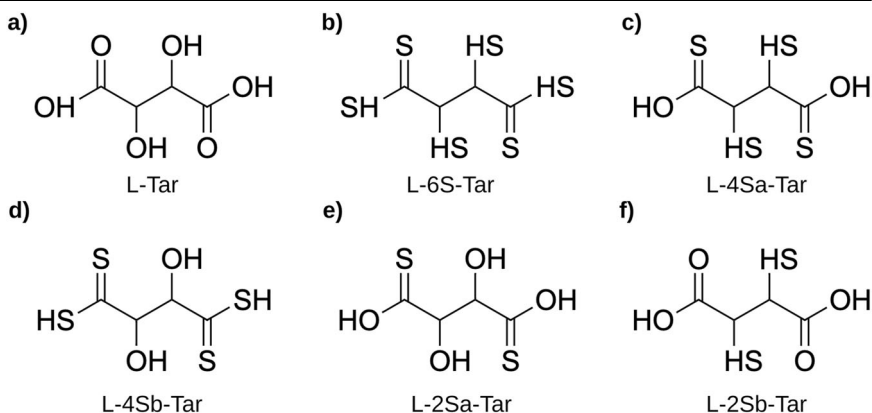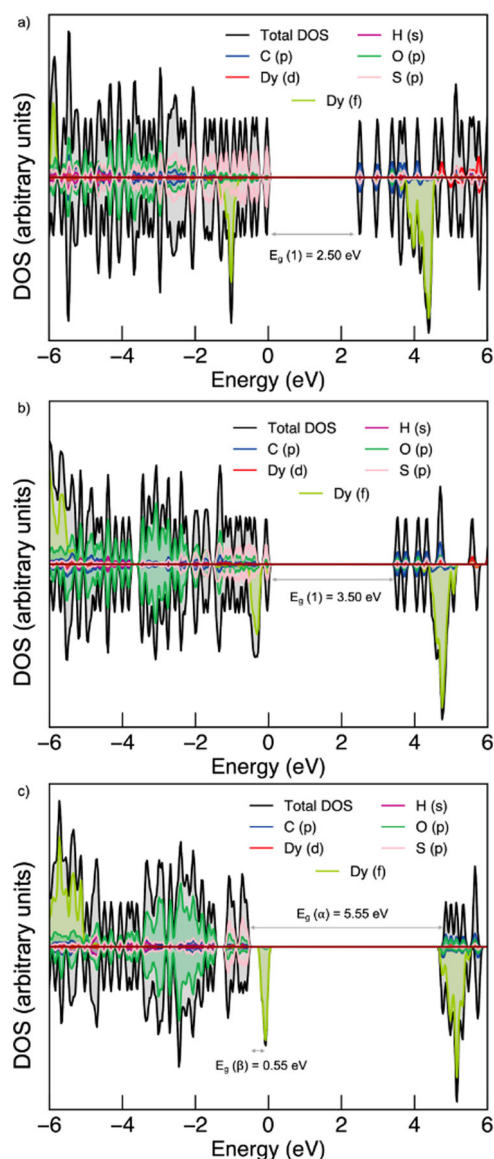
Fig. 4 | Projected density of states (PDOS) of 3D-Dy-L-4Sa-Tar, 3D-Dy-L-2Sa-Tar, and 3D-Dy-L-2Sb-Tar. The PDOS of these compounds are shown respectively in (**a–c**). The zero energy corresponds to the Fermi level. Alpha spin states are shown above the horizontal line, and beta-spin states are below. The projected DOS into the p states of C, d (f) states of Dy, s states of H, p states of S, p states of O and total states are shown in blue, red (yellow), magenta, pink, green, and black, respectively.

Methods

All the calculations were performed using PW-DFT with Projected Augmented Wave (PAW) potentials[39,40] implemented in the Vienna Ab initio Simulation Package (VASP)[41–44]. The geometry of the 3D Dy-L-Tar MOF was obtained from experimental X-ray crystallographic data deposited on the Cambridge Crystallographic Data Center (CCDC 1981576). Although lanthanide atoms are known to have open-shell configurations with large multiplicities, closed-shell configurations have been reported to yield almost identical geometries, which allows to save substantial computational time without compromising the accuracy[45,46]. Thus, the geometry of 3D Dy-L-Tar MOF was fully optimized using the PBE exchange-correlation functional[47], along with the Grimme's DFT-D3 scheme[48] for the dispersion interactions, and the f electrons of the Dy(III) cation included in the pseudopotential. Convergence for the geometry optimization under spin-restricted conditions was performed with a cut-off energy of 400 eV and a $2 \times 2 \times 1$ Γ-centered k points grid (see Supplementary Notes 2 and 3, Supplementary Figs. 2 and 3 and Supplementary Table 1).

The characterization of the electronic structure was carried out explicitly treating the f electrons of the lanthanide metal atom in a spin unrestricted fashion; this calculation was performed with the HSE06 hybrid functional, often reported as highly accurate for band gap energies in MOF materials[49–52]. Due to the large size of the unit cell of the Ln-MOF, the reciprocal space was sampled at the Γ point. Indeed, increasing the number of k points (from $1 \times 1 \times 1$ to $3 \times 3 \times 1$) did not result any significant change neither for the energy nor for the electronic states (see SI), in accordance with earlier works with MOFs[53]. Projected Density of States (PDOS) were plotted with Python script sumo[54] and molecular representations were done using the VESTA[55] software. The inclusion of SOC effects on the calculation has a negligible effect on the computed bandgap and DOS results of the material (see Supplementary Note 4), as expected from previous works[56–60]. Furthermore, we emphasize that the 3D Dy-L-Tar MOF (triclinic P-1 space group) has no symmetry, consequently no directional dependence on the electronic properties, namely, density of states and conductivity should be expected (isotropic material), see Supplementary Fig. 4.

Data availability

The authors declare that the data supporting the findings of this study are available within the paper and its Supplementary Information files. The cartesian coordinates of the studied compounds can be found in Supplementary Tables 3–7. Should any raw data files be needed in another format they are available from the corresponding author upon reasonable request. Source data are provided with this paper.

References

1. Varshney, P. & Agrawal, H. Spintronics technology: a review. *Natl. Conf. Adv. Technol. Appl. Sci.* (2014).
2. Mtangi, W. et al. Control of electrons' spin eliminates hydrogen peroxide formation during water splitting. *J. Am. Chem. Soc.* **139**, 2794–2798 (2017).
3. Ivanov, K. L., Wagenpfahl, A., Deibel, C. & Matysik, J. Spin-chemistry concepts for spintronics scientists spin-chemistry concepts for spintronics scientists. *Beilstein J. Nanotechnol.* **8**, 1427–1445 (2017).
4. Tsymbal, E. Y., Mryasov, O. N. & LeClair, P. R. Spin-dependent tunneling in magnetic tunnel junctions. *J. Phys. Cond. Matter* **15**, R109 (2003).
5. Waldeck, D. H. Chiral-induced spin selectivity effect. *J. Phys. Chem. Lett.* **3**, 2178–2187 (2012).
6. Michaeli, K., Kantor-Uriel, N., Naaman, R. & Waldeck, D. H. The electron's spin and molecular chirality-how are they related and how do they affect life processes? *Chem. Soc. Rev.* **45**, 6478–6487 (2016).

material and/or at its space-group chirality (helicity), is not an essential feature in order to exhibit a spin asymmetric display of the DOS near the fermi energy. In fact, such asymmetry arises exclusively from the f states of the dysprosium atom.

In addition, the investigation of the origin of the spin-filtering capacity of the 3D Dy-L-Tar MOF offers key features for the rational design of MOFs with enhanced electron conductivity and optimum spin-filtering properties. The substitution of the chemically hard oxygen atoms of the tartrate ligand by the chemically softer sulfur atoms results in an increased electronic conductivity, although at the risk of losing the spin asymmetry of the DOS around the Fermi energy, i.e., failing to keep the spin-filtering capacity. However, the substitution of a reduced number of sulfur atoms, i.e., thiolation of only the oxygens attached to the chiral centers of tartrate, is predicted to boost the conductivity of electrons of one of the spins, and simultaneously retain the structural integrity and spin-filtering capacity.

7. Zöllner, M. S., Varela, S., Medina, E., Mujica, V. & Herrmann, C. Insight into the origin of chiral-induced spin selectivity from a symmetry analysis of electronic transmission. *J. Chem. Theory Comput.* **16**, 2914–2929 (2020).

8. Maslyuk, V. V., Gutierrez, R., Dianat, A., Mujica, V. & Cuniberti, G. Enhanced magnetoresistance in chiral molecular junctions. *J. Phys. Chem. Lett.* **9**, 5453–5459 (2018).

9. Naaman, R., Paltiel, Y. & Waldeck, D. H. Chiral molecules and the electron spin. *Nat. Rev. Chem.* **3**, 250–260 (2019).

10. Huizi-Rayo, U. et al. An ideal spin filter: long-range, high-spin selectivity in chiral helicoidal 3-dimensional metal organic frameworks. *Nano Lett.* **20**, 8476–8482 (2020).

11. Göhler, B. et al. Spin selectivity in electron transmission through self-assembled monolayers of double-stranded DNA. *Science* **331**, 894–897 (2011).

12. Xie, Z. et al. Spin specific electron conduction through DNA oligomers. *Nano Lett.* **11**, 4652–4655 (2011).

13. Kettner, M. et al. Spin filtering in electron transport through chiral oligopeptides. *J. Phys. Chem. C.* **119**, 14542–14547 (2015).

14. Kettner, M. et al. Chirality-dependent electron spin filtering by molecular monolayers of helicenes. *J. Phys. Chem. Lett.* **9**, 2025–2030 (2018).

15. Bloom, B. P., Kiran, V., Varade, V., Naaman, R. & Waldeck, D. H. Spin selective charge transport through cysteine capped CdSe quantum dots. *Nano Lett.* **16**, 4583–4589 (2016).

16. Lu, H. et al. Spin-dependent charge transport through 2D chiral hybrid lead-iodide perovskites. *Sci. Adv.* **5**, 1–8 (2019).

17. Torres-Cavanillas, R. et al. Reinforced room-temperature spin filtering in chiral paramagnetic metallopeptides. *J. Am. Chem. Soc.* **142**, 17572–17580 (2020).

18. Ballesteros-Rivas, M. et al. Highly conducting coordination polymers based on infinite M(4,4′-Bpy) chains flanked by regular stacks of non-integer TCNQ radicals. *Angew. Chem. Int. Ed.* **50**, 9703–9707 (2011).

19. Avendano, C., Zhang, Z., Ota, A., Zhao, H. & Dunbar, K. R. Dramatically different conductivity properties of metal-organic framework polymorphs of Tl(TCNQ): an unexpected room-temperature crystal-to-crystal phase transition. *Angew. Chem. Int. Ed.* **50**, 6543–6547 (2011).

20. Li, W., Shi, J., Zhang, K. & MacManus-Driscoll, J. Defects in complex oxide thin films for electronics and energy applications: challenges and opportunities. *Mater. Horiz.* **7**, 2832–2859 (2020).

21. Zhang, W. B. et al. Stability and magnetism of vacancy in NiO: a GGA +U study. *Eur. Phys. J. B* **64**, 153–158 (2008).

22. Kalatarian, M. M., Asgari, S. & Mustarelli, P. A theoretical approach to evaluate the rate capability of Li-ion battery cathode materials. *J. Mater. Chem. A* **2**, 107 (2014).

23. Pastor, E. et al. Electronic defects in metal oxide photocatalysts. *Nat. Rev. Mater.* **7**, 503–521 (2022).

24. Yutong, N. et al. Electronic transport through EuO spin-filter tunnel junctions. *Phys. Rev. B* **86**, 205310 (2012).

25. Miao, G. & Moodera, J. Spin manipulation with magnetic semiconductor barriers. *Phys. Chem. Chem. Phys.* **17**, 751–761 (2015).

26. Miao, G., Chang, J., Assaf, B., Heiman, D. & Moodera, J. Spin regulation in composite spin-filter barrier devices. *Nat. Commun.* **5**, 3682 (2014).

27. Saffarzadeh, A. & Farghadan, R. A spin-filter device based on armchair graphene nanoribbons. *Appl. Phys. Lett.* **98**, 023106 (2011).

28. Schneider, C. M. & Kirschner, J. Magnetism at surfaces and in ultrathin films. *Handb. Surf. Sci.* **2**, 511–668 (2000).

29. Wrobel, F. et al. Doped NiO: the mottness of a charge transfer insulator. *Phys. Rev. B* **101**, 195128 (2020).

30. Karsthof, R., Grundmann, M., Anton, A. M. & Kremer, F. Polaronic interacceptor hopping transport in intrinsically doped nickel oxide. *Phys. Rev. B* **99**, 235201 (2019).

31. Adler, D. Electronic structure of amorphous semiconductors. *Phys. Rev. Lett.* **36**, 1197 (1976).

32. Reinert, F. et al. Electron and hole doping in NiO. *Z. Phys. B Condens. Matter* **97**, 83–93 (1995).

33. Yakout, S. M. Spintronics: future technology for new data storage and communication devices. *J. Supercond. Nov. Magn.* **33**, 2557–2580 (2020).

34. Jayendran, A. & Jayendran, R. Conductors, insulators and semiconductors. In *Englisch für Elektroniker, Viewegs Fachbücher der Technik* (eds Jayendran, A. & Jayendran, R.) 1–7 (Vieweg+Teubner Verlag, 1996).

35. Solazzo, M., O'Brien, F. J., Nicolosi, V. & Monahan, M. G. The rationale and emergence of electroconductive biomaterial scaffolds in cardiac tissue engineering. *APL Bioeng.* **15**, 041501 (2019).

36. Calahorro, A. J. et al. Rare earth anthracenedicarboxylate metal-organic frameworks: slow relaxation of magnetization of Nd3+, Gd3+, Dy3+, Er3+ and Yb3+ based materials. *Dalton Trans.* **45**, 591–598 (2016).

37. Xie, L. S., Skorupskii, G. & Dincă, M. Electrically conductive metal-organic frameworks. *Chem. Rev.* **120**, 8536–8580 (2020).

38. Kepp, K. P. A quantitative scale of oxophilicity and thiophilicity. *Inorg. Chem.* **55**, 9461–9470 (2016).

39. Joubert, D. From ultrasoft pseudopotentials to the projector augmented-wave method. *Phys. Rev. B Condens. Matter Mater. Phys.* **59**, 1758–1775 (1999).

40. Bloch, F. Über Die Quantenmechanik Der Elektronen in Kristallgittern. *Z. f.ür. Phys.* **52**, 555–600 (1929).

41. Kresse, G. & Hafner, J. Ab initio molecular dynamics for liquid metals. *Phys. Rev. B* **47**, 558 (1993).

42. Wien, T. U. & Hauptstrage, W. Ab initio molecular-dynamics simulation of the liquid-metal-amorphous-semiconductor transition in germanium. *Phys. Rev. B* **49**, 14251 (1994).

43. Kresse, G. & Furthmüller, J. Efficient iterative schemes for Ab initio total-energy calculations using a plane-wave basis set. *Phys. Rev. B Condens. Matter Mater. Phys.* **54**, 11169 (1996).

44. Kresse, G. & Furthmüller, J. Efficiency of Ab-initio total energy calculations for metals and semiconductors using a plane-wave basis set. *Comput. Mater. Sci.* **6**, 15–50 (1996).

45. Vogel, D. J., Nenoff, T. M. & Rimsza, J. M. Tuned hydrogen bonding in rare-earth metal-organic frameworks for design of optical and electronic properties: an exemplar study of γ-2,5-dihydroxyterephthalic acid. *ACS Appl. Mater. Interf.* **12**, 4531–4539 (2020).

46. Vogel, D. J., Sava Gallis, D. F., Nenoff, T. M. & Rimsza, J. M. Structure and electronic properties of rare earth DOBDC metal-organic-frameworks. *Phys. Chem. Chem. Phys.* **21**, 23085–23093 (2019).

47. Perdew, J. P. et al. Restoring the density-gradient expansion for exchange in solids and surfaces. *Phys. Rev. Lett.* **100**, 136406 (2008).

48. Grimme, S., Antony, J., Ehrlich, S. & Krieg, H. A consistent and accurate ab initio parametrization of density functional dispersion correction (DFT-D) for the 94 elements H-Pu. *J. Chem. Phys.* **132**, 154104 (2010).

49. Da Silva, J. L. F., Ganduglia-Pirovano, M. V., Sauer, J., Bayer, V. & Kresse, G. Hybrid functionals applied to rare-earth oxides: the example of ceria. *Phys. Rev. B Condens. Matter Mater. Phys.* **75**, 045121 (2007).

50. Garza, A. J. & Scuseria, G. E. Predicting band gaps with hybrid density functionals. *J. Phys. Chem. Lett.* **7**, 4165–4170 (2016).

51. Janesko, B. G., Henderson, T. M. & Scuseria, G. E. Screened hybrid density functionals for solid-state chemistry and physics. *Phys. Chem. Chem. Phys.* **11**, 443–454 (2009).

52. Butler, K. T., Hendon, C. H. & Walsh, A. Electronic chemical potentials of porous metal-organic frameworks. *J. Am. Chem. Soc.* **136**, 2703–2706 (2014).

53. Yang, L. M., Vajeeston, P., Ravindran, P., Fjellvåg, H. & Tilset, M. Revisiting isoreticular MOFs of alkaline earth metals: a comprehensive

study on phase stability, electronic structure, chemical bonding, and optical properties of A-IRMOF-1 (A = Be, Mg, Ca, Sr, Ba). *Phys. Chem. Chem. Phys.* **13**, 10191–10203 (2011).

54. M Ganose, A., J Jackson, A. & O Scanlon, D. Sumo: command-line tools for plotting and analysis of periodic Ab initio calculations. *J. Open Source Softw.* **3**, 717 (2018).

55. Momma, K. & Izumi, F. VESTA 3 for three-dimensional visualization of crystal, volumetric and morphology data. *J. Appl. Crystallogr.* **44**, 1272–1276 (2011).

56. Wen, X. et al. Effect of spin-orbit coupling on the actinide dioxides AnO_2 (An=Th, Pa, U, Np, Pu and Am): a screened hybrid density functional study. *J. Chem. Phys.* **137**, 154707 (2012).

57. Larson, P., Lambrecht, R., Chantis, A. & Van Schilfgaarde, M. Electronic structure of rare-earth nitrides using LSDA+U approach: importance of allowing 4f orbitals to break the cubic crystal symmetry. *Phys. Rev. B* **75**, 045114 (2007).

58. Uzunok, H., Tutuncu, H. & Bagci, S. The effect of spin-orbit coupling on the physical and superconducting properties of the Ir-rich cubic Laves superconductors Air_2 (A=Y, Lu and Th). *J. Phys. Chem. Solids* **174**, 111169 (2023).

59. Pandey, S. et al. Electronic structures and magnetism of Zr-, Th-, and U-based metal-organic frameworks (MOFs) by density functional theory. *Comput. Mater. Sci.* **184**, 109903 (2020).

60. Uzunok, H., Tutuncu, H., Srivastava, G., Ipsara, E. & Basoglu, A. The effect of spin orbit interactions on the physical properties of La $TSi3$ (T=Ir, Pd and Rh): first-principles calculations. *J. Appl. Phys.* **121**, 193904 (2017).

Author contributions

X.G. performed and analyzed the calculations, J.M.U. and E.S.S. brought the inspiration and supervised the work, E.S.S. and G.E.P. performed the experimental measurements, E.J.-I. analyzed the calculations and supervised the work. All the authors contributed to the writing of the work. All authors reviewed the manuscript. All authors have given approval to the final version of the manuscript.

Competing interests

The authors declare no competing interests.

Additional information

Supplementary information The online version contains supplementary material available at https://doi.org/10.1038/s42005-024-01651-4.

Correspondence and requests for materials should be addressed to Eider San Sebastian or Elisa Jimenez-Izal.

Peer review information *Communications Physics* thanks Dayton Vogel and the other, anonymous, reviewer(s) for their contribution to the peer review of this work.

Reprints and permissions information is available at http://www.nature.com/reprints

Publisher's note Springer Nature remains neutral with regard to jurisdictional claims in published maps and institutional affiliations.